Published in final edited form as:
J Surg Res. 2014 August ; 190(2): 528–534. doi:10.1016/j.jss.2014.05.012.

FLUORESCENT-TILMANOCEPT FOR TUMOR MARGIN ANALYSIS IN THE MOUSE MODEL

Ava Hosseini, MD[1], **Jennifer Baker, MD**[1], **Christopher Tokin, MD**[1], **Zhengtao Qin, MS**[2,3], **David Hall, PhD**[2,3,4], **Dwayne Stupak, PhD**[4,5], **Tomoko Hayashi, MD, PhD**[4,5], **Anne Wallace, MD**[1,4], and **David Vera, PhD**[2,3,4]

[1]Department of Surgery, University of San Diego, California

[2]Department of Radiology, University of San Diego, California

[3]In Vivo Cancer and Molecular Imaging Center, University of San Diego, California

[4]Moores Cancer Center, University of San Diego, California

[5]Department of Reproductive Medicine, University of San Diego, California

Abstract

Background—Dendritic cells (DC) are localized in close proximity to cancer cells in many well-known tumors, and thus may be a useful target for tumor margin assessment.

Materials and Methods—[^{99m}Tc]-Cy7-tilmanocept was synthesized and in vitro binding assays to bone marrow-derived DC were performed. Fifteen mice, implanted with either 4T1 mouse mammary or K1735 mouse melanoma tumors, were administered 1.0 nmol of [^{99m}Tc]-Cy7-tilmanocept via tail vein injection. After fluorescence imaging 1 or 2 hours post-injection, the tumor, muscle, and blood were assayed for radioactivity to calculate percent injected dose (%ID). Digital images of the tumors after immunohistochemical staining for DC were analyzed to determine DC density.

Results—In vitro binding demonstrated subnanomolar affinity of [^{99m}Tc]-Cy7-tilmanocept to DC (K_D=0.31±0.11nM). After administration of [^{99m}Tc]-Cy7-tilmanocept, fluorescence imaging

To whom manuscript correspondence should be addressed: David R. Vera, PhD, UCSD Moores Cancer Center, 3855 Health Sciences Drive 0987, La Jolla, CA 92093-0987, Phone: (858) 822-2574, Fax: (858) 822-6194, dvera@ucsd.edu.

DISCLOSURES: Dr. David Vera is the inventor of tilmanocept.

Ava Hosseini, MD–analysis and interpretation, writing the article
Jennifer Baker, MD–data collection, analysis and interpretation, article revision
Christopher Tokin, MD– data collection
Zhengtao Qin, MS–data collection, article revision
David Hall, PhD–conception and design, analysis and interpretation, article revision
Dwayne Stupak, PhD–analysis and interpretation
Tomoko Hayashi, MD, PhD–data collection
Anne Wallace, MD–conception and design, analysis and interpretation, article revision, funding
David Vera, PhD–conception and design, analysis and interpretation, article revision, funding

showed a 5.5 fold increase in tumor signal as compared to pre-injection images and a 3.3 fold difference in fluorescence activity when comparing the tumor to the surgical bed after tumor excision. Immunohistochemical staining analysis demonstrated that DC density positively correlated with tumor %ID/g (r=0.672, p=0.03) and higher DC density was observed at the periphery versus center of the tumor (186±54K vs. 64±16K arbitrary units, p=0.001).

Conclusions—[^{99m}Tc]-Cy7-tilmanocept exhibits in vitro and in vivo tumor-specific binding to DC and may be useful as a tumor margin targeting agent.

Keywords

Tilmanocept; Lymphoseek; Dendritic Cells; Tumor Margins; Fluorescence Imaging

INTRODUCTION

Dendritic cells (DC) play a critical role in immunity through capturing and processing antigens, migrating to lymphoid organs, and activating T and B lymphocytes [1]. Through this same process, they promote anti-neoplastic activity; studies have shown that higher numbers of tumor-infiltrating dendritic cells (TIDC) correlate with improved prognosis [1, 2]. Some human tumors, such as breast cancer, have a considerable amount of TIDC [3, 4], whereas other tumors such as renal cell carcinoma have poor infiltration [5]. Similarly, murine models have shown varying amounts of TIDC depending on tumor type, with the mammary 4T1 [6] and the melanoma K1735 [7] murine tumor models showing numerous TIDC.

Due to the propensity of DC to infiltrate breast cancer, TIDC may be a useful marker for determining tumor margins intraoperatively. Mature DC found specifically along the tumor periphery in human breast cancer further supports the use of TIDC as a potential tumor margin target [8]. Assessing tumor margins in the operating room in modern breast surgery is suboptimal, with frozen section analysis of margins resulting in a re-excision rate around 20% [9, 10]. Positive margins are associated with higher cancer recurrence rates after breast conservation therapy [11], and therefore more accurate methods of identifying tumor margins intraoperatively are needed. One such approach may be to target TIDC owing to their infiltration of and peripheral distribution within breast tumors.

Tilmanocept, also known as diethylenetriaminepentaacetic acid (DTPA)-mannosyl-dextran and Lymphoseek (Navidea Biopharmaceuticals, Dublin, OH), is a radiopharmaceutical that exhibits specific binding to mannose-binding protein receptor present on some immune cells derived from the mononuclear phagocytic lineage (MPS), from which DC arise. It is a synthetic molecule composed of a dextran backbone with multiple mannose units that serve as receptor recognition sites as well as DTPA units that can be labeled for molecular detection. [12, 13]

Our group has previously published subnanomolar binding affinity of tilmanocept to macrophages, but the binding potential to DC has not been studied. The purpose of this study is to determine the in vitro and in vivo binding capacity of [^{99m}Tc]-Cy7-tilmanocept to

DC using nuclear and fluorescence detection and to determine its utility in tumor margin analysis.

MATERIALS AND METHODS

Tilmanocept was provided by Navidea Biopharmaceuticals. The authors of this study had full control over the inclusion of all data and information submitted for publication. This study was approved by the Institutional Animal Care and Use Committee of the University of California, San Diego.

Fluorescence- and Radio-labeling of Tilmanocept

The conjugation of cyanine 7 (Cy7) to the dextran backbone of tilmanocept was performed in a manner previously described [14, 15]. Purity was confirmed by size exclusion (TSKgel G2000SWx1; Tosoh Bioscience LLC, Tokyo, Japan) HPLC (System Gold; Beckman Coulter, Inc., Brea, CA) using 0.9% saline as the mobile phase [16]. The eluate was monitored by UV absorbance and fluorescence (L-7480; Hitachi America, Ltd., Farmington Hills, MI). The fluorescence purity of all preparations was in excess of 98%. Estimation of Cy7 density was defined as the average number of Cy7 molecules per tilmanocept molecule [15]. The resultant density was 2 molecules of Cy7 per tilmanocept molecule. Radiolabeling of Cy7-tilmanocept was performed using a tin reduction method [15]. Figure 1 shows the structure of [^{99m}Tc]-Cy7-tilmanocept.

[^{99m}Tc]-Cy7-Tilmanocept In Vitro Binding Assays

C57BL/6 bone marrow-derived dendritic cells (BMDC) were prepared as described previously [17]. One hundred twenty million immature BMDC were separated into 5 vials of 24 million cells each. The final concentration was 4.8 million cells per 0.1 mL of solution, and the final ligand concentrations were 0.0625, 0.125, 0.375, 0.75, and 15 nmol/L. Each ligand-cell mixture was vortexed, incubated on ice for 1 hour, and vortexed again. Next, four tubes for every ligand concentration were made by combining 0.1 mL of ligand-cell mixture with 0.15 mL of a 4:1 mixture of silicon fluid 550 and mineral oil. Tubes were centrifuged (Microfuge E; Beckman Coulter, Inc., Brea, CA) for 30 seconds. The bound fraction, assumed to be within the cell pellet, was separated from the free fraction by cutting through the oil layer and assayed separately for gamma radiation (Gamma 9000; Beckman Coulter, Inc., Brea, CA). Each stock ligand concentration had 0.05 mL taken for a standard measurement. The equilibrium disassociation constant (K_D) was estimated using LIGAND software [18] and the resulting regression presented as a Scatchard plot [19]. This protocol was performed at 4°C to eliminate the effect of receptor recycling. The mean and standard deviation of triplicate measurements are reported.

4T1 Cell Culture and Tumor Implantation

Ten 6-week-old female BALB/c mice and five 6-week-old female B6C3F1 (weight range 18–27g) were purchased from Charles River Laboratories. All of the mice were of the same gender to minimize any variables that could potentially influence results. The mice were given a weeklong acclimation period prior to tumor implantation. The 4T1 cell line originated from a female Balb/c mouse mammary tumor and was gifted from the Stupack

Lab [20]. The K1735 cell line originated from an inbred C3H/HeN murine melanoma tumor [21] and was gifted from the Huard Lab (Geneva University Medical Center). Cells were grown in Dulbecco's Modified Eagle Medium (DMEM) solution with 10% Fetal Bovine Serum (FBS). On the day of tumor implantation, the 4T1 tumor cell suspension and the K1735 tumor cell suspension were prepared to a concentration of 8 million cells/mL and 2.4 million cells/mL, respectively. 0.25 mL of each suspension was drawn up into 1 mL syringes and placed on ice. All mice were anesthetized by inhalation of 2% isoflurane. Under anesthesia, one hind leg of each mouse was shaved and cleaned with alcohol, and 0.25 mL cell suspension (2 million 4T1 tumor cells or 600,000 K1735 tumor cells) was injected subcutaneously in this region. Tumors were grown over a period of 14 days for the 4T1 cell line and 20 days for the K1735 cell line.

In Vivo Optical Imaging

All mice were deemed ready for [^{99m}Tc]-Cy7-tilmanocept injection based on tumor size (volume range 60–609 mm^3). Under anesthesia, each mouse underwent tail vein injection of 1.0 nmol (0.1 mL, 250 μCi) of [^{99m}Tc]-Cy7-tilmanocept. Each mouse was imaged using a 758 nm excitation laser and 782 nm emission detection (Optix MX2 ART/GE) prior to injection and at 1 or 2 hours post-injection. Five of the 4T1-bearing mice were imaged at 1 hour and five at 2 hours. The K1735-bearing mice were imaged at 1 hour. Animals were euthanized after fluorescence images were obtained. The B6C3F1 mice underwent additional fluorescence imaging of the surgical bed alongside the excised tumor and excised muscle from the opposite hind leg. The fluorescence images were viewed using standard software (Optiview) and analyzed by drawing a circular region of interest (ROI) around each tumor to determine maximum fluorescence count. Each ROI encircled a 1×1 mm^2 pixel area.

Ex Vivo Nuclear Counts and Calculation of % ID per gram

Tumor, blood, and muscle from the hind leg opposite the tumor were removed and placed in separate plastic scintillation vials. Radioactivity was assayed for each of these three entities for each animal with a gamma counter using a 100–200 keV window (Gamma 9000; Beckman Coulter, Inc., Brea, CA). Each sample was compared with a counting standard prepared from a known dilution of [^{99m}Tc]-Cy7-tilmanocept. The amount of [^{99m}Tc]-Cy7-tilmanocept within each scintillation vial was expressed as percentage of injected dose (%ID) of [^{99m}Tc]-Cy7-tilmanocept per gram of tissue, which was calculated by comparing the radioactivity in each vial to the radioactivity in the counting standard.

Pathology and Immunohistochemical Analysis

After radioactivity counts were obtained, the tumor from each mouse was submitted to pathology as frozen blocks embedded in Optimal Cutting Temperate (OCT) compound (Sakura, Torrance, CA). Tumors were stained for DC using DC-specific integrin Cd11c antibody [22] purchased from BD Pharmingen. Digital images were taken of each 4T1 tumor slice using ×20 objective on the light microscope and SPOT basic software. Images were taken both at the center of the tumor tissue and the periphery. Each image was analyzed using the magic wand method as described in other studies [23] to determine the density of DC expressed as the immunocytochemical (ICC) index in arbitrary units.

Statistical Analysis

The Student's two-tailed *t* test and the Wilcoxon test (JMP, version 9, 2010; SAS Institute, Cary, NC) were used to compare %ID/g of tumor versus muscle and DC density in the tumor periphery versus center. A *P* value of less than 0.05 was considered significant. The Pearson correlation coefficient was used to determine the correlation of %ID/g of tumor to the ICC index of each tumor using the average of the central and peripheral tumor ICC indices for each specimen.

RESULTS

Subnanomolar binding affinity to dendritic cells

Figure 2 displays a representative Scatchard plot [19]. The mean dissociation constant (K_D) for this experiment was 0.19±0.19nM. Three binding assays yielded a mean K_D of 0.31±0.11nM.

Fluorescence Imaging and %ID shows tumor uptake of [^{99m}Tc]-Cy7-tilmanocept

Figure 3 shows representative fluorescence images of a BALB/c mouse with increased peak activity from pre-injection to post-injection of [^{99m}Tc]-Cy7-tilmanocept. In Figure 4, fluorescence activity is shown after removal of the tumor in a representative B6C3F1 mouse, with little fluorescence in the surgical bed or the muscle excised from the opposite hind leg as compared to high peak activity in the excised tumor. The peak fluorescence values for the tumor, muscle, and surgical bed for this mouse are 119.7, 30.7, and 29.4 kc·sec^{-1}·μwatts^{-1}, respectively. The peak fluorescence activity is 4.1 times greater in the tumor than the surgical bed in this example, and for the five B6C3F1 mice undergoing ex vivo tumor imaging, the mean ratio of tumor to surgical bed peak fluorescence activity is 3.3±2.0 kc·sec^{-1}·μwatts^{-1}.

The percent of injected dose per gram (%ID/g) measurements demonstrated increased amounts of [^{99m}Tc]-Cy7-tilmanocept in tumor tissue as well. 4T1 tumors imaged at 1 hour showed 1.76±0.36 %ID/g versus 0.40±0.20 %ID/g in muscle excised from the opposite hind leg ($p<0.001$) and 6.7±6.4 %ID/g in the blood. The five 4T1-bearing mice euthanized at 2 hours post-injection exhibited 1.06±0.25 %ID/g in the tumor versus 0.22±0.13 %ID/g in muscle (p<;0.001) and1.33±0.17 %ID/g in the blood. The K1735-bearing mice had 1.09±0.21 %ID/g in the tumors versus 0.27±0.08 %ID/g in muscle ($p<0.001$). Blood contained 2.08 ±0.91 %ID/g.

Immunohistochemistry shows increased DC density at tumor margins and a positive correlation between DC density and %ID/g

Figure 5 shows Cd11c staining of 4T1 tumor tissue to identify DC. Density of DC was found to be greater in the tumor periphery versus the center (186±54K versus 64±16K arbitrary units, p=0.001). DC density also positively correlated with %ID/g with a pearson correlation coefficient of 0.672 (Figure 6).

DISCUSSION

The purpose of this study was to determine the binding affinity of [^{99m}Tc]-Cy7-tilmanocept to DC and to determine the intratumoral binding of our probe in a mouse tumor model. In our in vitro studies, we found subnanomolar binding affinity of tilmanocept to BMDC, signifying avid binding. Prior studies have investigated the receptor-binding capacity of our probe to mannose-binding protein on J774E macrophages and similar subnanomolar binding was observed [15]. However, this is the first study to report DC binding affinity. Like macrophages, DC are known to express mannose-binding protein and this likely explains the observed specific binding.

To evaluate in vivo intratumoral binding characteristics, both fluorescence and radioactive labeling was used to measure tumor uptake of our probe after intravenous injection. Fluorescence imaging studies showed a 5.5 fold increase in tumor signal when comparing pre- and post-injection images, indicating localization of our probe. Additionally, after tumor excision, there was 3.3 fold greater peak fluorescence activity in the tumor as compared to the surgical bed. Similarly, ex vivo nuclear counts showed uptake of the probe by the tumor with a significant 4.5 fold greater amount of injected dose present in the tumor when compared with muscle from the opposite hind leg, signifying tumor-specific uptake of the radiopharmaceutical.

On pathology, DC density positively correlated with percent of injected dose. These results further corroborate the binding of [^{99m}Tc]-Cy7-tilmanocept to TIDC. Given that we found TIDC to be significantly more concentrated at the periphery of tumor sections as compared to the center, [^{99m}Tc]-Cy7-tilmanocept may be valuable as a probe in tumor margin analysis.

One major limitation of this study is the small sample size, and further experiments should be conducted with larger sample sizes to corroborate this data. The small sample size is especially evident in the K1735 tumor group with five mice, giving a large standard deviation when comparing peak fluorescence activity of the excised tumor to that of the surgical bed. One mouse in this group was an outlier with high fluorescence activity in the surgical bed as well as in the excised tumor, possibly signifying tumor tissue left behind. The other four mice, however, all had at least 3 fold higher peak fluorescence activity in the tumor as compared to the surgical bed. In future experiments, histochemical analysis of tumor margins should also be performed to compare to imaging data. Overall, however, this pilot study shows that [^{99m}Tc]-Cy7-tilmanocept binds to DC found in higher concentrations at the tumor periphery, and therefore its potential as tumor margin targeting agent should be further explored.

This application of [^{99m}Tc]-Cy7-tilmanocept would be especially useful in managing breast cancer in the operating room. Breast conservation therapy has become the treatment standard for most breast tumors. However, it has limitations: it is difficult to assess tumor margins in the operating room as evidenced by the 20–40% positive margin rate [24] and additional surgery is necessary if residual tumor is left behind. To avoid this high re-excision rate, improved techniques of intraoperative breast tumor margin assessment are needed.

Molecular imaging technologies are increasingly being used to analyze cancers, with rapid growth in the field of in vivo fluorescence imaging [25]. Near-infrared (NIR) fluorescence dyes like Cy7 have high tissue penetration and low autofluorescence, making them ideal for use in the operating room [26]. Advances in fluorescence imaging have already been applied to intraoperative tumor detection in other areas of oncology [27]. Specifically, clinical trials have shown promising results using fluorescence imaging in the detection of both primary liver lesions [28] and colorectal metastases to the liver [29]. Fluorescence imaging has also been applied to parathyroid adenoma identification with positive outcomes [30].

Although fluorescence imaging has not yet been used for human breast cancer management outside of sentinel node mapping, in vivo studies in the rat model have been effective in detecting tumor margins with intraoperative NIR fluorescence imaging systems [31]. Similar methods can be applied to intraoperative human breast cancer tumor analysis using Cy7-tilmanocept. After intravenous injection of Cy7-tilmanocept up to 24 hours prior to surgery, handheld intraoperative NIR fluorescence imaging systems can be used to demarcate the margins of the tumor. After tumor excision, the optical system can also be used to evaluate the surgical bed for any remaining fluorescence activity potentially could signify residual tumor.

Before TIDC can be used for tumor margin detection in breast cancer, further research should be directed towards better understanding their role in the tumor environment. For example, there is great variability in the number of TIDC from one breast cancer patient to the next [32]. Iwamoto et al. showed that increased amounts of certain types of TIDC are associated with earlier stage breast cancers [33]. Targeting this subtype of TIDC for margin identification may prove beneficial, because patients with early stage cancer are candidates for breast conservation therapy; therefore, these patients would most benefit from [^{99m}Tc]-Cy7-tilmanocept as a margin targeting agent. Those patients with more advanced cancer are more likely to require mastectomy without the need for intraoperative margin analysis. Another way to overcome the variability in number of TIDC is to develop methods to increase the number of TIDC in the tumor, such as through high-intensity focused ultrasound [8]. Finally, the increased number of DC in other inflammatory conditions, such as autoimmune diseases, poses another potential limitation in using TIDC to identify tumor margins. Further research should focus on determining if these states interfere with [^{99m}Tc]-Cy7-tilmanocept TIDC binding.

Acknowledgments

The authors thank Dr. Derek Emerson for his assistance in performing the in vitro binding assays.

References

1. Banchereau J, Steinman RM. Dendritic cells and the control of immunity. Nature. 1998; 392:245. [PubMed: 9521319]
2. Suzuki A, Masuda A, Nagata H, et al. Mature dendritic cells make clusters with T cells in the invasive margin of colorectal carcinoma. The Journal of pathology. 2002; 196:37. [PubMed: 11748640]
3. Thomachot MC, Bendriss-Vermare N, Massacrier C, et al. Breast carcinoma cells promote the differentiation of CD34+ progenitors towards 2 different subpopulations of dendritic cells with

CD1a(high)CD86(−)Langerin- and CD1a(+)CD86(+)Langerin+ phenotypes. International journal of cancer Journal international du cancer. 2004; 110:710. [PubMed: 15146561]

4. Bell D, Chomarat P, Broyles D, et al. In breast carcinoma tissue, immature dendritic cells reside within the tumor, whereas mature dendritic cells are located in peritumoral areas. The Journal of experimental medicine. 1999; 190:1417. [PubMed: 10562317]
5. Vicari AP, Caux C, Trinchieri G. Tumour escape from immune surveillance through dendritic cell inactivation. Seminars in cancer biology. 2002; 12:33. [PubMed: 11926410]
6. Norian LA, Rodriguez PC, O'Mara LA, et al. Tumor-infiltrating regulatory dendritic cells inhibit CD8+ T cell function via L-arginine metabolism. Cancer research. 2009; 69:3086. [PubMed: 19293186]
7. Preynat-Seauve O, Schuler P, Contassot E, et al. Tumor-infiltrating dendritic cells are potent antigen-presenting cells able to activate T cells and mediate tumor rejection. Journal of immunology. 2006; 176:61.
8. Xu ZL, Zhu XQ, Lu P, et al. Activation of tumor-infiltrating antigen presenting cells by high intensity focused ultrasound ablation of human breast cancer. Ultrasound in medicine & biology. 2009; 35:50. [PubMed: 18950932]
9. Cendan JC, Coco D, Copeland EM 3rd. Accuracy of intraoperative frozen-section analysis of breast cancer lumpectomy-bed margins. Journal of the American College of Surgeons. 2005; 201:194. [PubMed: 16038815]
10. Wilke LG, Brown JQ, Bydlon TM, et al. Rapid noninvasive optical imaging of tissue composition in breast tumor margins. American journal of surgery. 2009; 198:566. [PubMed: 19800470]
11. Singletary SE. Surgical margins in patients with early-stage breast cancer treated with breast conservation therapy. American journal of surgery. 2002; 184:383. [PubMed: 12433599]
12. Vera DR, Wallace AM, Hoh CK, et al. A synthetic macromolecule for sentinel node detection: (99m)Tc-DTPA-mannosyl-dextran. Journal of nuclear medicine : official publication, Society of Nuclear Medicine. 2001; 42:951.
13. Wallace AM, Hoh CK, Ellner SJ, et al. Lymphoseek: a molecular imaging agent for melanoma sentinel lymph node mapping. Annals of surgical oncology. 2007; 14:913. [PubMed: 17146742]
14. Vera DR, Hall DJ, Hoh CK, et al. Cy5.5-DTPA-galactosyl-dextran: a fluorescent probe for in vivo measurement of receptor biochemistry. Nuclear medicine and biology. 2005; 32:687. [PubMed: 16243643]
15. Emerson DK, Limmer KK, Hall DJ, et al. A receptor-targeted fluorescent radiopharmaceutical for multireporter sentinel lymph node imaging. Radiology. 2012; 265:186. [PubMed: 22753678]
16. Qin Z, Hall DJ, Liss MA, et al. Optimization via specific fluorescence brightness of a receptor-targeted probe for optical imaging and positron emission tomography of sentinel lymph nodes. Journal of biomedical optics. 2013; 18:101315. [PubMed: 23958947]
17. Datta SK, Redecke V, Prilliman KR, et al. A subset of Toll-like receptor ligands induces cross-presentation by bone marrow-derived dendritic cells. Journal of immunology. 2003; 170:4102.
18. Munson PJ, Rodbard D. Ligand: a versatile computerized approach for characterization of ligand-binding systems. Analytical biochemistry. 1980; 107:220. [PubMed: 6254391]
19. Scatchard G. The attractions of proteins for small molecules and ions. Annals of the New York Academy of Sciences. 1949; 51:660.
20. Walsh C, Tanjoni I, Uryu S, et al. Oral delivery of PND-1186 FAK inhibitor decreases tumor growth and spontaneous breast to lung metastasis in pre-clinical models. Cancer biology & therapy. 2010; 9:778. [PubMed: 20234193]
21. Fidler IJ, Gruys E, Cifone MA, et al. Demonstration of multiple phenotypic diversity in a murine melanoma of recent origin. Journal of the National Cancer Institute. 1981; 67:947. [PubMed: 6944560]
22. del Hoyo GM, Martin P, Vargas HH, et al. Characterization of a common precursor population for dendritic cells. Nature. 2002; 415:1043. [PubMed: 11875574]
23. Lehr HA, Mankoff DA, Corwin D, et al. Application of photoshop-based image analysis to quantification of hormone receptor expression in breast cancer. The journal of histochemistry and cytochemistry : official journal of the Histochemistry Society. 1997; 45:1559. [PubMed: 9358857]

24. Pleijhuis RG, Graafland M, de Vries J, et al. Obtaining adequate surgical margins in breast-conserving therapy for patients with early-stage breast cancer: current modalities and future directions. Annals of surgical oncology. 2009; 16:2717. [PubMed: 19609829]
25. Weissleder R, Pittet MJ. Imaging in the era of molecular oncology. Nature. 2008; 452:580. [PubMed: 18385732]
26. Frangioni JV. New technologies for human cancer imaging. Journal of clinical oncology : official journal of the American Society of Clinical Oncology. 2008; 26:4012. [PubMed: 18711192]
27. Kokudo, N.; Ishizawa, T., editors. Fluorescent Imaging: Treatment of Hepatobiliary and Pancreatic Diseases, S. Kargar AG; Tokyo, Japan: 2013.
28. Ishizawa T, Fukushima N, Shibahara J, et al. Real-time identification of liver cancers by using indocyanine green fluorescent imaging. Cancer. 2009; 115:2491. [PubMed: 19326450]
29. van der Vorst JR, Schaafsma BE, Hutteman M, et al. Near-infrared fluorescence-guided resection of colorectal liver metastases. Cancer. 2013; 119:3411. [PubMed: 23794086]
30. van der Vorst JR, Schaafsma BE, Verbeek FP, et al. Intraoperative near-infrared fluorescence imaging of parathyroid adenomas with use of low-dose methylene blue. Head & neck. 2013
31. Mieog JS, Hutteman M, van der Vorst JR, et al. Image-guided tumor resection using real-time near-infrared fluorescence in a syngeneic rat model of primary breast cancer. Breast cancer research and treatment. 2011; 128:679. [PubMed: 20821347]
32. Lespagnard L, Gancberg D, Rouas G, et al. Tumor-infiltrating dendritic cells in adenocarcinomas of the breast: a study of 143 neoplasms with a correlation to usual prognostic factors and to clinical outcome. International journal of cancer Journal international du cancer. 1999; 84:309. [PubMed: 10371352]
33. Iwamoto M, Shinohara H, Miyamoto A, et al. Prognostic value of tumor-infiltrating dendritic cells expressing CD83 in human breast carcinomas. International journal of cancer Journal international du cancer. 2003; 104:92. [PubMed: 12532424]

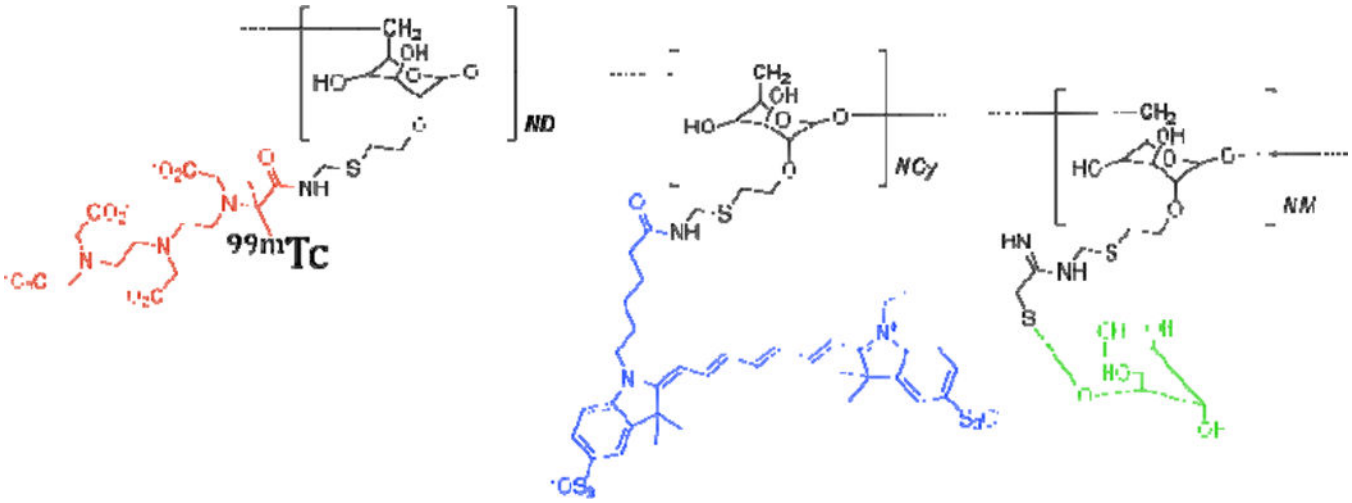

Figure 1.
[^{99m}Tc]-Cy7-tilmanocept with technetium-99m (red), cyanine 7 (blue), and mannose-binding receptor (green).

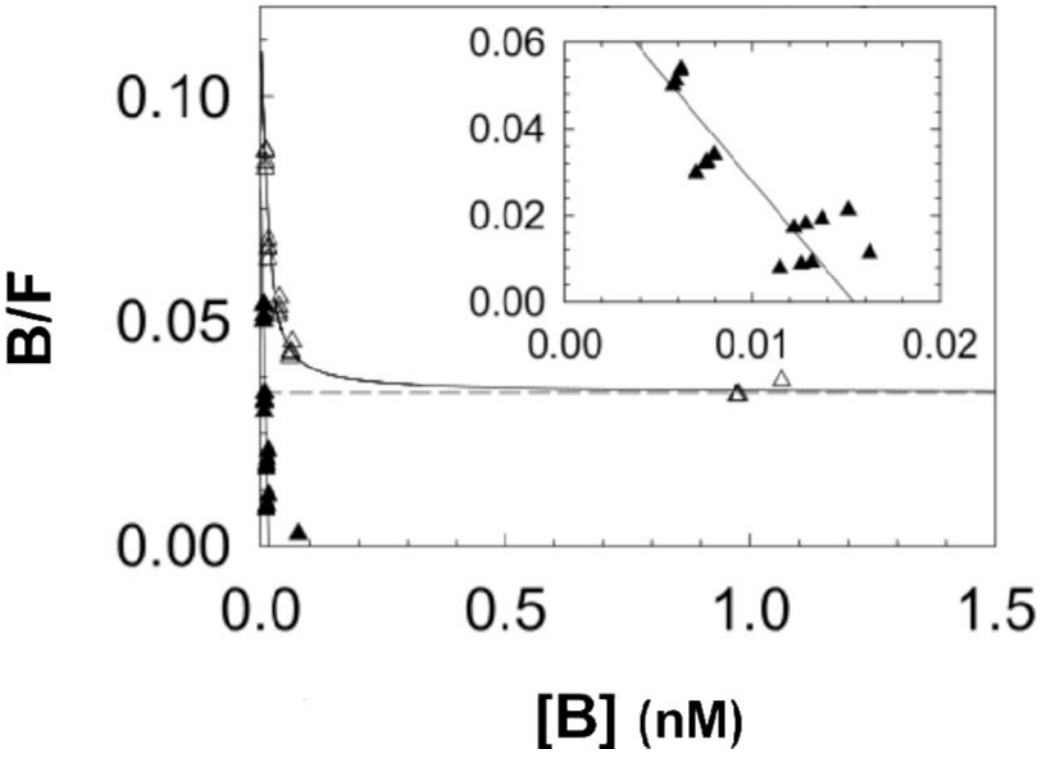

Figure 2.

The Scatchard plot shows results of a single in vitro binding experiment analyzed with LIGAND software [18], which separates the specific-(▲) and nonspecific-bound (△) radioactivity prior to estimation of a dissociation constant (K_D). Inset shows expanded view of the specific-bound component used to calculate the K_D, which was 0.19±0.19nM (negative slope of straight solid line). Mean K_D of the three in vitro binding assays was 0.31±0.11nM.

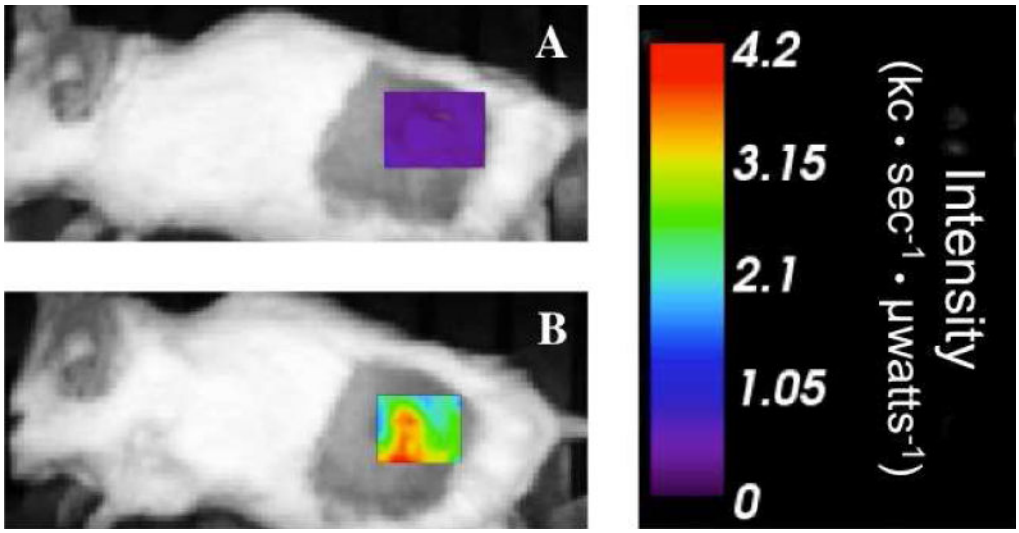

Figure 3.

Fluorescence images of a BALB/c mouse with a 4T1 tumor acquired 1 hour post-injection show increased peak intensity (kilocounts·sec^{-1}·$\mu watts^{-1}$) from pre-injection (A) to post-injection (B) of tail vein injection of 1.0 nmol [^{99m}Tc]-Cy7-tilmanocept.

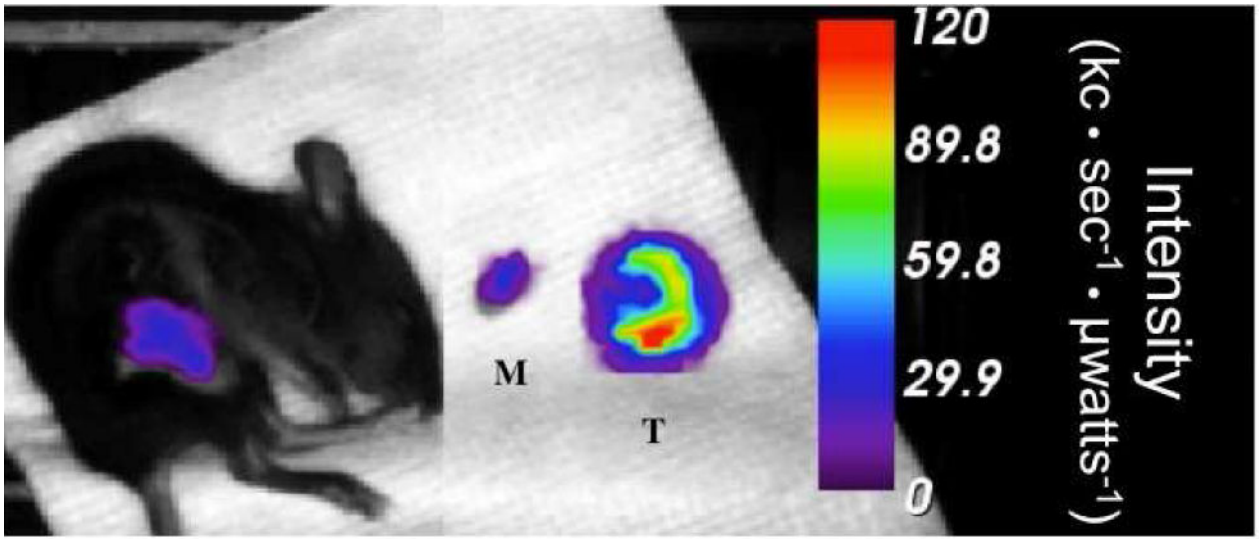

Figure 4.

After excision of the K1735 tumor in a B6C3F1 mouse, peak fluorescence activity in the surgical bed is 29.4 kc·sec·$^{-1}$·µwatts^{-1}. Similarly, muscle (M) excised from the opposite hind leg has 30.7 kc·sec^{-1}·µwatts^{-1} peak fluorescence activity versus 119.7 kc·sec^{-1}·µwatts^{-1} in the tumor (T). The mouse was euthanized 1 hour after injection of fluorescent-labeled tilmanocept.

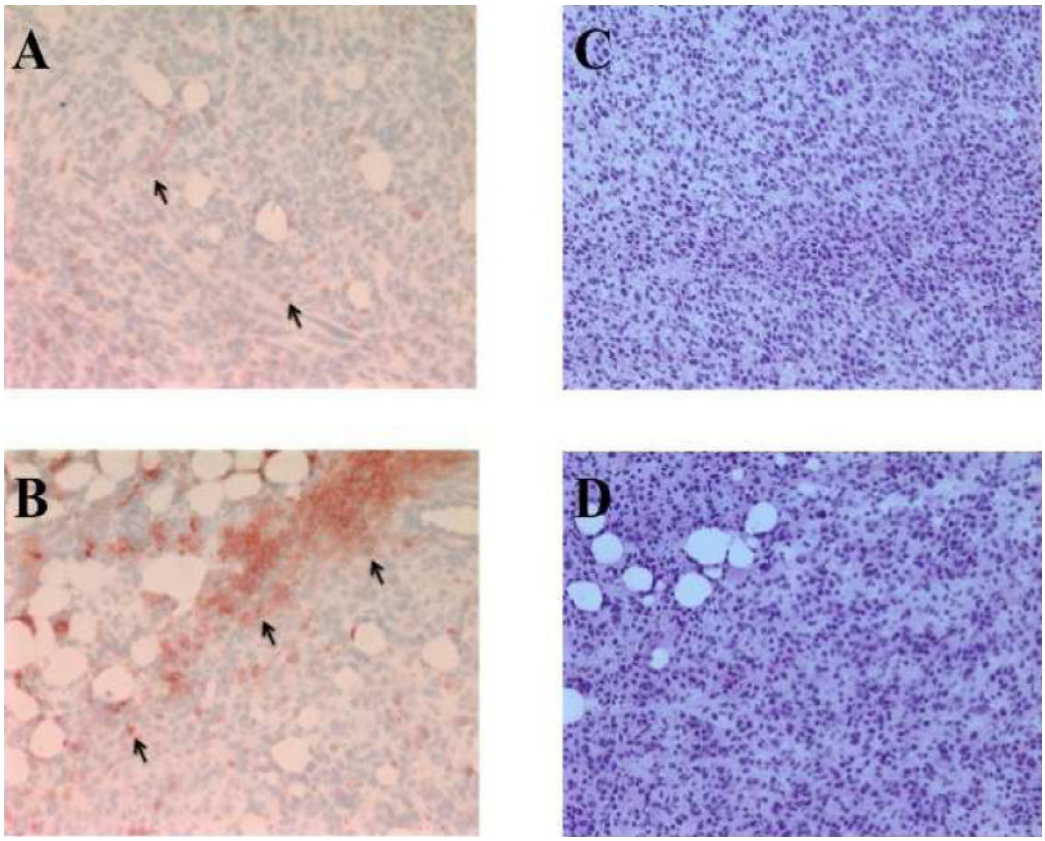

Figure 5.

Cd11c staining of dendritic cells (arrows) within 4T1 tumor tissue in red. A) Central tumor shows less dendritic cell density than B) tumor periphery (15521 versus 162618 arbitrary units). Standard H&E staining of central tumor (C) and peripheral tumor (D) is shown for comparison.

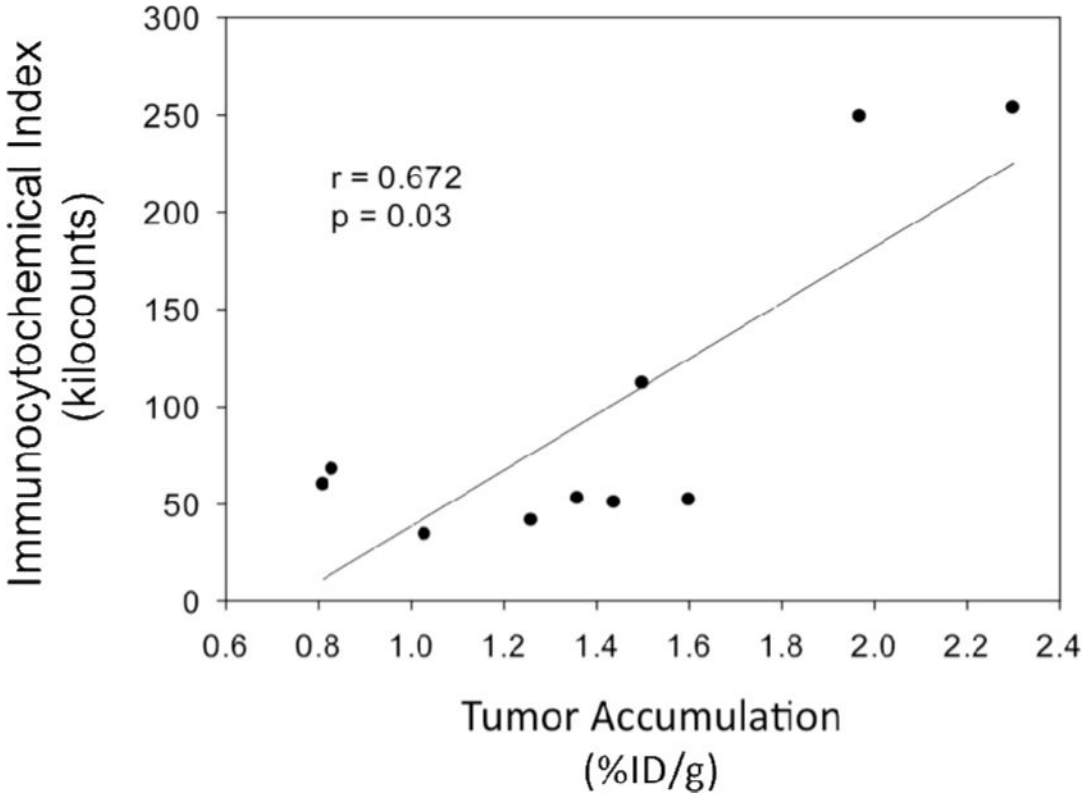

Figure 6.

Density of dendritic cells based on immunocytochemical index analysis shows a positive correlation with [^{99m}Tc]-Cy7-tilmanocept tumor accumulation (r=0.672, p=0.03).